

DESIGN ANALYSIS OF NEW METAMATERIAL FOR EM ABSORPTION REDUCTION

M. R. I. Faruque^{1,2}, M. T. Islam^{1,*}, and N. Misran^{1,2}

¹Institute of Space Science (ANGKASA), Universiti Kebangsaan Malaysia, UKM, Bangi, Selangor 43600, Malaysia

²Department of Electrical, Electronic and Systems Engineering, Faculty of Engineering and Built Environment, Universiti Kebangsaan Malaysia, UKM, Bangi, Selangor 43600, Malaysia

Abstract—A new triangular metamaterials (TMMs) is designed for electromagnetic (EM) absorption reduction at microwave frequencies in this paper. The reduction of EM absorption with a new TMMs attachment is investigated in this research. The finite-difference time-domain method with lossy-Drude model is adopted in this investigation. The method of EM reduction is presented and the effects of position, distance, and size of metamaterials are analyzed. TMMs have achieved a 1.0923 W/kg for SAR 1 gm which is 45.44% reduction of the initial SAR value for the case of 1 gm SAR.

1. INTRODUCTION

The public awareness concerning the health hazards has been mounting, which carries an augmented obligation on electromagnetic (EM) absorption reduction for cellular phones with the more widespread use of mobile phones. The basic parameter in the electromagnetic (EM) absorption is defined in terms of the specific absorption rate (SAR), or the absorbed power in unit mass of tissue [1–4]. The interaction of mobile handset antennas with the human body is a large consideration in mobile communications. The user's body, in particular the head and hand, persuade the antenna voltage standing wave ratio (VSWR), gain, and radiation patterns. Moreover, thermal effects, as tissues are uncovered to unlimited electromagnetic energy, can be a solemn health hazard. Consequently standards organizations have set revelation restrictions in terms of SAR [1–8]. SAR is used

Received 23 November 2011, Accepted 9 January 2012, Scheduled 16 January 2012

* Corresponding author: Mohammad Tariqul Islam (titareq@yahoo.com).

to measure revelation to fields between 100 kHz and 10 GHz [9–12]. It is frequently used to measure power absorbed from cellular phones and during MRI scans. The value will depend on the geometry of the ingredient of the body that is uncovered to the RF energy and on the accurate location and geometry of the RF source.

Cellular handset protection and the enforcement of relevant exposure standards are issues in the recent media, and regulatory agencies are aggravated to promise that acquiescence testing is satisfactory. IEEE Standard 1528 [1] and IEC 62209-1 specify protocols and procedure for the measurement of the peak spatial-average SAR induced within a simplified model of the head of users of hand held radio transceivers (cellular phones). For example, the SAR limit specified in IEEE C95.1: 1999 is 1.6 W/kg in a SAR 1 gm averaging mass while that précised in IEEE C95.1: 2005 has been reorganized to 2 W/kg in a 10 gm averaging mass [1, 2]. This new SAR limit précised in IEEE C95.1: 2005 is equivalent to the limit specified in the International Commission on Non-Ionizing Radiation Protection (ICNIRP) guidelines.

The interaction of the mobile handset with the human head has been explored by a lot of published papers allowing for; first, the consequence of the human head on the handset antenna performance counting the feed-point impedance, gain, and efficiency [13], and second, the collision of the antenna EM radiation on the user's head due to the absorbed power, which is measured by predicting the induced SAR in the head tissue [13–17].

In [16, 18] a perfect electric conductor (PEC) reflector was sited between a human head and the driver of a folded loop antenna. The result showed that the radiation efficiency can be improved and the peak SAR value can be condensed. In [17], a study on the belongings of attaching conductive materials to cellular phone for SAR reduction has been offered. It is publicized that the position of the shielding material is a significant factor for SAR reduction effectiveness. There is a requirement to make an endeavor for reducing the spatial peak SAR in the design phase of the metamaterial because the likelihood of a spatial peak SAR above the recommended exposure limit cannot be entirely ruled out.

Metamaterials signify artificially constructed materials having electromagnetic properties not usually found in nature. Two important parameters, dielectric permittivity (ϵ) and magnetic permeability (μ) collectively determine the response of any materials and metamaterials to the electromagnetic wave. Typically, ϵ and μ are both positive in ordinary materials. The negative permittivity can be obtained by arranging the metallic thin wires periodically [18–25]. Alternatively,

an array of split ring resonators (SRRs) can display negative effective permeability. In [9], the calculated SRRs operated at 1.8 GHz were used to condense the SAR value in a lossy material. The metamaterials are calculated on circuit board so it perhaps easily incorporated to the cellular phone. Simulation of wave propagation into metamaterials was proposed in [9, 18]. The authors utilized the FDTD method with lossy-Drude models for metamaterials simulation. This technique is a supportive approach to study the wave propagation characteristics of metamaterials [13] and has been further developed with the perfectly matched layer (PML) and extended to three-dimension problem [6].

Since 2000, the rate of publications on electromagnetic-metamaterials has grown exponentially [12, 25–29], indicative of the extreme interest that artificial materials have generated. In particular, the harms to be solved in SAR reduction require a correct depiction of the cellular phone, anatomical depiction of the head, alignment of the phone and the head, and appropriate design of metamaterials. In the beginning materials are sited between the antenna and a human head, and then replaced by a metamaterial. In order to study the SAR reduction of an antenna operated at the GSM 900 band, the effectual medium parameter of metamaterials is put to be negative at 900 MHz. Different positions, sizes, and negative medium parameters of metamaterials for SAR reduction efficacy are also analyzed.

In this paper, we focus on artificial structures to design TMMs that is attached on PCB with mobile phones to reduce SAR in human head. This paper is structured as follows. Section 2 describes the numerical investigation of the handset collectively among the SAM phantom head, and the FDTD method is used with positive meshing techniques for speedy and accurate investigation. Impacts on SAR of metamaterial attachment in human head are also analyzed in Section 2. Section 3 describes the new design of triangular split ring resonators (TSRRs) structure, design and simulation of metamaterials results are explained in Section 4, and Section 5 concludes the paper.

2. METAMATERIAL ATTACHMENT IN HUMAN HEAD

The handset and the SAM phantom head is considered for this simulation study that is provided by Computer Simulation Technology Microwave Studio (CST MWS). The PIFA type of antenna is included in the simulation model. A complete handset model composed of the circuit board, LCD display, keypad, battery, and housing was used for simulation. The electrical properties of materials considered for calculation are listed in Table 1. A PIFA antenna constructed in a helical sense operating at 900 MHz for GSM application was considered

Table 1. Electrical properties of materials considered for calculation.

Phone Materials	ϵ_r	σ (S/m)
Circuit Board	4.4	0.05
Housing Plastic	2.5	0.005
LCD Display	3.0	0.02
Rubber	2.5	0.005
SAM Phantom Head		
Shell	3.7	0.0016
Liquid @ 900 MHz	40	1.42

in the simulation model. The minimum and maximum mesh sizes were 0.3 mm and 1.0 mm used in this calculation. A total no. of 2,122,164 mesh cells were produced for the complete model, and the complete simulation time was 1208 seconds (including mesh generation) for each run on an Intel Core TM 2 Duo E 8400 3.0 GHz CPU with 4 GB RAM system.

Antenna radiation and its interaction with the head tissues using the FDTD method from the CST MWS Electromagnetic software is utilized in this paper. A portable telephone model at 900 MHz for the present study is as shown in Fig. 1. It was well thought-out to be a quarter wavelength PIFA antenna mounted on a rectangular conducting box. The conducting box was 10 cm tall, 4 cm wide, and 3 cm thick. The PIFA antenna was situated at the top surface of the conducting box.

The FDTD method was employed in the numerical analysis. Its discretized formulations were derived from the following Maxwell's time-domain equations:

$$\frac{\delta H}{\delta t} = -\frac{1}{\mu_0 \mu'_r} (\nabla \times E) - \frac{\sigma^*}{\mu_0 \mu'_r} H \quad (1)$$

$$\frac{\delta E}{\delta t} = -\frac{1}{\epsilon_0 \epsilon'_r} (\nabla \times H) - \frac{\sigma}{\epsilon_0 \epsilon'_r} E \quad (2)$$

where $\sigma^* = \omega \mu_0 \mu''_r$ and $\sigma = \omega \epsilon_0 \epsilon''_r$. A space domain enclosing the human head and the phone model is also shown in Fig. 1. The time step was set to $\delta/\sqrt{3c}$, where c is the speed of light, to guarantee the numerical stability. The time-stepping was performed for about eight sinusoidal cycles in order to reach a stable state. The head models considered in this study were obtained from a MRI-based head model through the whole brain Atlas website. Six types of tissues, i.e., bone, brain, muscle, eye ball, fat, and skin were involved in this model [9, 29]. Numerical simulations of SAR value were performed by FDTD method.

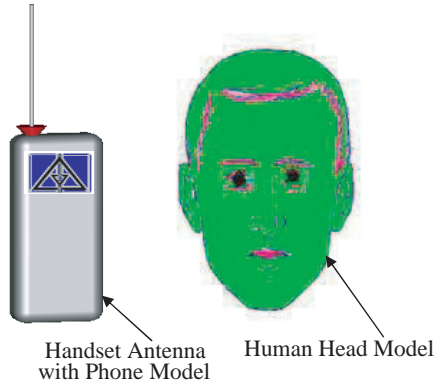


Figure 1. Human head and phone model for SAR computation.

The parameters for FDTD calculation were as follows in this paper. The simulation domain was $128 \times 128 \times 128$ cells. The cell sizes were set as $\Delta x = \Delta y = \Delta z = 1$ mm. The computational domain was terminated with 8 cells perfect matched layer (PML). A PIFA antenna was modeled by thin-wire approximation.

In this section, the designed TSRRs were placed between the antenna and a human head thus reducing the SAR value. In order to study SAR reduction of an antenna operated at the GSM 900 band, different positions, sizes, and metamaterials for SAR reduction effectiveness are also analyzed by using the FDTD method in conjunction with a human head model.

The dispersive models for all the dielectrics were adopted during the simulation in order to accurately characterize the TSRRs. The antenna was arranged in parallel to the head axis, the distance is varied from 5 mm to 20 mm, and finally 20 mm was chosen for comparison with the metamaterials. Besides that, the output power of the mobile phone model needs to be set before SAR is simulated. In this paper, the output power of the cellular phone is 600 mW at the operating frequency of 900 MHz. In the real case, the output power of the mobile phone will not exceed 250 mW for normal use, while the maximum output power can reach to 1 W or 2 W is far away from the mobile station (cellular phone). The SAR simulation is compared with the results in [3, 9, 17] for validation, as shown in Table 2. The calculated peak SAR 1 gm value is 2.002 W/kg, and SAR 10 gm value is 1.293 W/kg when the phone model is placed 20 mm away from the human head model without a metamaterial. This SAR reduction is better than without metamaterials attachment, the result reported in [3, 17], which is 2.17 W/kg and 2.28 W/kg, for SAR 1 gm. This is

Table 2. Comparisons of without metamaterial peak SAR at 900 MHz.

Tissue	SAR value (W/kg)
SAR 1 gm value for [3]	2.17
SAR 1 gm value for [9]	2.43
SAR 1 gm value for [17]	2.28
SAR 1 gm value this work	2.002

since the mobile antenna position, and antenna sizes are not properly situated and antenna is different also. This SAR value is better compared with the result reported in [9], which is 2.43 W/kg for SAR 1 gm. This is achieved using different radiating powers and different antenna.

The distance among the antenna feeding point and periphery of the metamaterials was $A = 3$ mm. The size of the metamaterials in the xz plane was $45 \text{ mm} \times 45 \text{ mm}$ and the thickness was 6 mm. The SAR value and antenna performance with the metamaterial were scrutinized. To assess the power radiated from the antenna, the source impedance (Z_S) was assumed to be identical to the composite conjugate of the free space radiation impedance ($Z_S = 105.18 + j81.97 \Omega$). The source voltage (V_S) was preferred to acquire a radiated power in free space equal to 600 mW ($V_S = \sqrt{0.6 \cdot 8 \cdot R_{RO}}$). When analyzing the consequence of the metamaterials and the human head on the antenna performance, the source impedance and source voltage were predetermined at the Z_S and V_S values.

The power radiated from the antenna was appraised by comparing the radiation impedance in this situation ($Z_R = R_R + jX_R$) and used the following [18] equation:

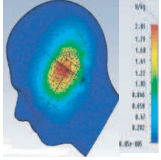
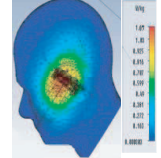
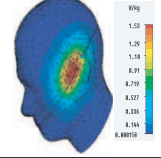
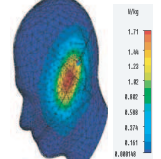
$$P_R = \frac{1}{2} V_S^2 \frac{R_R}{|Z_R + Z_S|^2}. \quad (3)$$

The total power immersed in the head was calculated by

$$P_{abs} = \frac{1}{2} \int_V \sigma |E|^2 dv. \quad (4)$$

Different negative medium parameters for EM absorption reduction effectiveness were analyzed in this research. We sited negative permittivity mediums among the antenna and the human head. First, the plasma frequencies of the mediums were set to be $\omega_{pe} = 9.239 \times 10^9$ rad/s, which provide mediums with $\mu = 1$ and $\varepsilon = -3$ at 900 MHz. The mediums with bigger negative permittivity $\mu = 1$, and $\varepsilon = -5$; $\mu = 1$, and $\varepsilon = -7$ were also analyzed. We set $\Gamma_e = 1.22 \times 10^8$ rad/s, signifying the mediums have sufferers. Numerical results of antenna

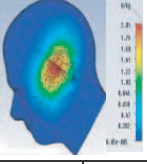
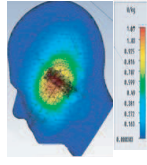
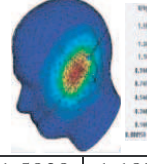
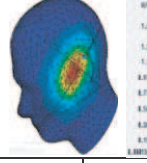
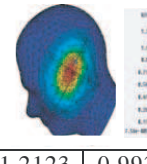
Table 3. Antenna performances and SAR reduction at 900 MHz using metamaterial.

	$Z_R (\Omega)$	P_R (mW)	P_{abs} (mW)	Peak head SAR (W/kg)	
				1 gm	10 gm
Without material	$63.39 + j94.53$	600	268.83		
				2.002	1.673
$\mu = 1, \epsilon = -3$	$51.04 + j98.94$	512.7	206.83		
				1.0724	0.8215
$\mu = 1, \epsilon = -5$	$53.84 + j94.75$	528.7	234.43		
				1.5387	1.1555
$\mu = 1, \epsilon = -7$	$58.74 + j96.05$	539.6	248.73		
				1.712	1.293

performance and SAR value are given in Table 3. The peak SAR 1 gm becomes 1.07 W/kg with $\mu = 1$ and $\epsilon = -3$ mediums and impedance is pretentious by metamaterials. Compared to the situation without metamaterials, the radiated power is condensed by 14.55% whereas the SAR is condensed by 46.44%. With the use of and mediums, the SAR diminution efficiency is decreased. Though the radiated power from the antenna is fewer affected. Comparisons of the EM absorption reduction effectiveness with different positions and sizes of metamaterials were analyzed. Simulation results are shown in Table 4.

In case 1, the distance among the antenna and metamaterial was changed from 2 mm to 6 mm. In case 2, the metamaterial thickness was

Table 4. Antenna performances and SAR values by using different positions and different sizes of metamaterial.

	$Z_R (\Omega)$	P_R (mW)	P_{abs} (mW)	Peak head SAR (W/kg)	
				1 gm	10 gm
Without material	$63.39+j94.53$	600	268.83		
				2.002	1.673
$\mu=1,$ $\epsilon=-3$	$51.04+j98.94$	512.7	206.83		
				1.0724	0.8215
Case 1	$57.73+j95.15$	532.8	249.43		
				1.5939	1.1973
Case 2	$61.35+j96.37$	555.3	254.21		
				1.6538	1.2433
Case 3	$68.63+j105.87$	571.65	213.98		
				1.2123	0.9934

abridged from 6 mm to 2 mm. It is found that both the peak SAR 1 gm and power absorbed by the head enhance with the increase of distance or the decrease of thickness. In case 3, the size of the metamaterial was augmented from 45 mm \times 45 mm to 56 mm \times 56 mm. It can be noted that the peak SAR 1 gm is abridged significantly whereas

the awful conditions on the radiated power due to metamaterial is inconsequential. To additional examine whether the metamaterial affected the antenna performance or not, the radiation pattern of the PIFA antenna with the $\mu = 1$ and $\varepsilon = -3$ metamaterial was analyzed.

It is publicized that there is a great influence of the distance between the antenna and metamaterial on SAR reduction. If the distance between the antenna and metamaterial is augmented from 2mm to 6mm, then the SAR value also increases from 0.73 to 1.07 W/kg for SAR 10 gm and 1.16 to 1.61 W/kg for SAR 1 gm respectively. This is because the dielectric constant, conductivity, density and magnetic tangent losses conductivity are also varied. Additionally, it can be observed that the SAR value increases with the decrease of the thickness of metamaterial. In addition, the SAR value reduces speedily when metamaterial size is large 45 mm \times 45 mm to 56 mm \times 56 mm subsequently the SAR value also reduces from 1.21 to 0.81 W/kg for the cases of SAR 10 gm and 1.62 to 1.23 W/kg for SAR 1 gm.

To study the consequence of SAR reduction with the use of new TMMs, the radiated power from the PIFA antenna with $\mu = 1$ and $\varepsilon = -3$ mediums was fixed at 600 mW. Compared results are shown in Table 5. It is found that calculated SAR value at 900 MHz, without the metamaterial, is 2.002 W/kg for SAR 1 gm and with the metamaterial, the reduction of the SAR 1 gm value is 1.096 W/kg. The reduction is 45.44% where as the design reported in [9] achieved 22.63%. This is achieved due to the contemplation of different density, different antenna, and different size of metamaterial and different type of conductivity. The SAR reduction is improved that our previous research (where we achieved about 42.12%) [29], due to the use of new TMMs. In the TMMs design we have considered 28 elements in the propagation direction which will reduce the thickness and metamaterial size. Furthermore, the size of the mobile phone was considered 61 mm but in our previous paper it was considered 63 mm.

Table 5. Effects of comparisons with metamaterials on SAR reduction ($P_R = 0.5$ W for 900 MHz).

	900 MHz	
	Without material	$\mu = 1, \varepsilon = -3$
SAR 1 gm value for [9]	2.43	1.89
SAR 1 gm value for [29]	2.002	1.1623
SAR 1 gm value in this work	2.002	1.0963

From simulation results, the metamaterials can condense peak SAR effectively and the antenna performance can be less affected. The metamaterials are resonant due to internal capacitance and inductance. The mediums will exhibit a stop band with a single negative medium parameter. Moreover, we necessitate being more careful in taking the square root of negative μ and ε of metamaterial. For example, instead of writing, $\varepsilon = -3$ we write $\varepsilon = 3 \exp(i\pi)$. As soon as the mediums with $\mu = 1$ and $\varepsilon = -3$ are studied, the propagation constant becomes

$$\beta = \omega \sqrt{\mu \varepsilon \mu_0 \varepsilon_0} = \omega \sqrt{3 \mu_0 \varepsilon_0} \times \exp(i\pi/2) = \omega \sqrt{3 \mu_0 \varepsilon_0}. \quad (5)$$

The propagation constant is imaginary and the fields inside the metamaterials will fall off exponentially with the distance from the surface.

3. ANALYSIS OF SAR USING TSRRS

The SAR in the head is abridged by placing the TMMs among the antenna and the human head. The TMMs is on a scale less than the operating wavelength. The structures are resonant due to internal capacitance and inductance. The stop band can be calculated at the operation bands of mobile phone radiation. The TMMs are designed on a printed circuit board so it may be effortlessly integrated to the mobile phone. By arranging sub-wavelength resonators sporadically we get the TMMs structure.

We establish that the TMMs can be used to decrease the peak SAR 1 gm and SAR 10 gm in the head from the FDTD investigation. In this section, the TMMs are operated at the 900 and 1800 MHz bands of the cellular phone were considered. The TMMs can be attained by arranging TSRRs sporadically. The TSRRs structure consists of two concentric triangular ring of conductive material. There is a gap on each triangular ring, and each triangular ring is located opposite to the gap on the other ring. The schematics of the TSRRs structure that we used in this study as shown in Fig. 2.

To construct the TMMs for SAR reduction, we proposed one model of resonators namely the TSRRs as shown in Fig. 2. We design the resonators for operation at the 900 MHz bands. The TSRRs contains two triangular rings, each with gaps appearing on the opposite sides [9]. The SRRs was introduced by Pendry et al. in 1999 [11] and subsequently used by Smith et al. for synthesis of the first left-handed artificial medium [12, 30–33]. We design the metamaterials from sporadically arrangement of SRRs to condense the SAR value. By correctly designing structure parameters of TSRRs, the effectual medium parameter can be negative around 900 and 1800 MHz band.

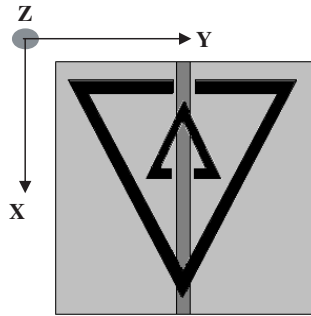


Figure 2. The structure of the TSRRs.

In Fig. 2, the structures of resonators are defined by the subsequent structure parameters: the triangular ring thickness c , the triangular ring gap d , the triangular ring size l , the split gap g , and c_0 is the speed of light in free space. The resonant frequency ω is very sensitive to little changes in the structure parameters of TSRRs. The frequency response can be scaled to higher or lower frequency by correctly choosing these geometry parameters by utilizing the following equation [29].

$$\omega^2 = \frac{3lc_0^2}{\pi \ln \frac{2c}{dr^3}} \quad (6)$$

The TSRRs is resonating at approximately half the guided-wavelength of the resonant frequency. There are two resonances from the split rings. We have given the formula for the resonance of the outer split ring, which has a lower resonance frequency.

4. RESULTS AND DISCUSSION

Numerical simulations that forecast the transmission properties depend on the assorted structure parameters of this system. Simulations of this complex structure are executed with the FDTD method. Fig. 3 shows the top view of plane wave episode on the periodic TSRRs which construct the resonators for SAR reduction. Periodic boundary conditions are used to decrease the computational domain and an absorbing boundary condition is used at the propagation regions. The total-field/scatter-field formulation is used to agitate the plane wave. The regions within the computational domain and outside of the TSRRs were assumed to be vacuums.

To verify our FDTD simulation, the structure parameters of TSRRs were chosen the same as [25]. The structure parameters were $d = g = c = 0.33$ mm, and $l = 3$ mm. The thickness and dielectric constant of the circuit board were 0.45 and 4.4 mm, respectively. The

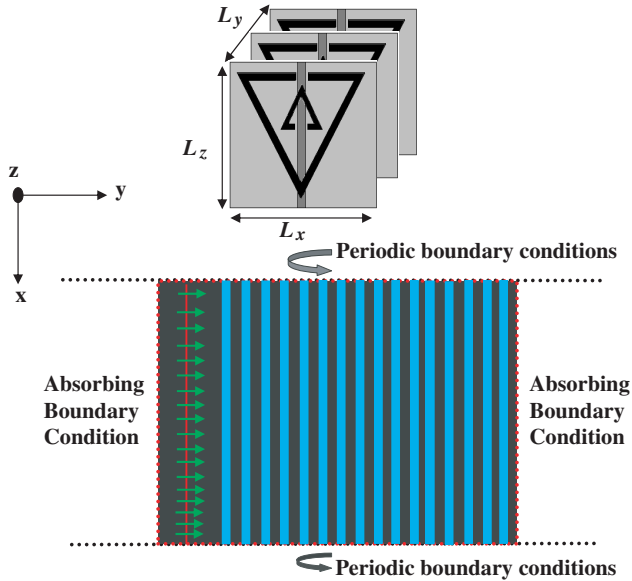


Figure 3. Top sight of a plane wave incident on the periodic TSRRs.

unit elements in the propagation direction were 28 elements. Periodic boundary conditions were applied normal to the propagation direction. In [25], the measured results show that the SRRs display a stop band extending from 8.1 to 9.5 GHz, but in our simulation results show that the TSRRs exhibit a stop band extending from 8.3 to 9.4 GHz which is appears similar to our simulation results. This is because the ring of SRRs was considered in that paper was square sizes but in our paper the TSRRs already modified and developed a new TMMs shape. Fig. 4 shows simulated transmission spectra of TSRRs. The stop band is shifted toward higher frequency band and extends from 17 to 24.5 GHz. From this study, it is found that both of the two incident polarizations can produce stop band.

As shown in the stop band corresponds to a region where either permittivity or permeability is negative. When the magnetic field is polarized along the split ring axes H_{\parallel} , it will produce a magnetic field that may either oppose or enhance the incident field. A large capacitance in the region between the rings will be generated and the electric field will be strongly concentrated. There is strong field coupling between TSRRs and the permeability medium will be negative at stop band. On the other hand, the behavior of the stop band can be contrasted with that occurring for the H^{\perp} case. Because the magnetic field is parallel to the plane of the TSRRs, we assume the magnetic effects are small, and that permeability is small, positive,

and slowly varying. In the H^\perp condition, these structures can be viewed as arranging the metallic wires periodically. The continuous wires behave like high-pass filter, which means the permittivity can be negative below the plasma frequency [34,35]. For this metallic wire structures, there will be a stop band around the resonance frequency. As shown in Fig. 4, a stop band occurs, but outside of the stop band region of the H_\parallel polarization. The contrast between the two stop bands in the H^\perp and H_\parallel cases illustrates the difference between the magnetic and electric responses of the TSRRs. Theoretical investigations in have shown that the H_\parallel band gap is due to negative permeability and the H^\perp band gap is due to negative permittivity.

From this study, it is found that both of the two incident polarizations can produce a stop band. As shown in the stop band corresponds to a region where either the permittivity or permeability is negative. When the magnetic field is polarized along the split ring axes, it will produce a magnetic field that may either oppose or enhance the incident field.

The stop bands of the TSRRs are designed to be at 900 MHz and 1800 MHz. The periodicity along x , y , z axes are $L_x = 61$ mm, $L_y = 1.5$ mm, and $L_z = 61$ mm respectively. On the other hand, to obtain a stop band at 1800 MHz, the parameters of the TSRRs are chosen as $c = 1.8$ mm, $d = 0.6$ mm, $g = 0.6$ mm, and $r = 12.7$ mm. The periodicity along the x , y , z axes are $L_x = 50$ mm, $L_y = 1.5$ mm, and $L_z = 50$ mm, respectively. Both the thickness and dielectric constant

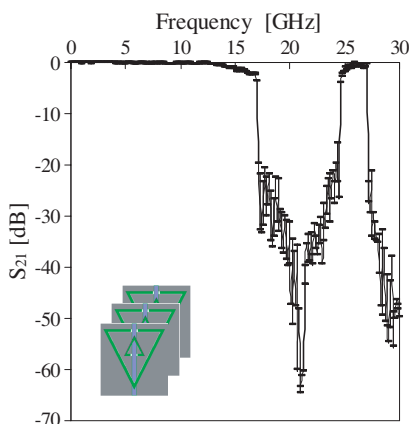


Figure 4. Modeled transmission spectra of the TSRRs in the xz plane.

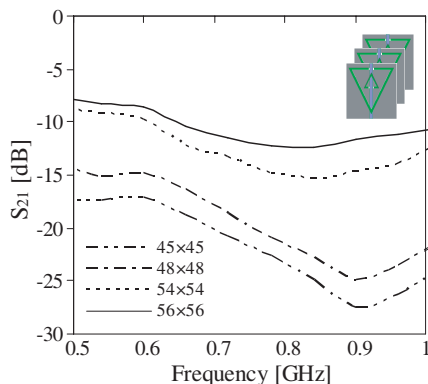


Figure 5. Modeled transmission spectra of the designed TSRRs for different dimension at 900 MHz.

of the circuit boards for 900 MHz and 1800 MHz are 0.508 mm and 3.38 respectively. After properly choosing geometry parameters, the TSRRs medium can display a stop band around 900 MHz and 1800 MHz.

The model transmission spectra for dissimilar structure dimension of the TSRRs as shown in Fig. 5. From the Fig. 5, it can be evidently seen that, the resonant frequency f is very sensitive to little changes in the structure dimensions of the TSRRs.

We have tried to use a high impedance surface configuration to reduce the peak SAR. However, we found that when these structures operate at 900 MHz, the sizes of these structures are too large for cellular phone application. A negative permittivity medium can also be constructed by arranging the metallic thin wires periodically. However, we found that when the thin wires operate at 900 MHz, the size is also too large for practical application. Because the TSRRs structures are significant due to internal capacitance and inductance, they are on a scale less than the wavelength of radiation. In this study, it is established that the TSRRs can be designed at 900 MHz while the size is similar to that of a cellular phone.

5. CONCLUSION

The EM absorption among an antenna and the human head with new TMMs has been discussed in this paper. Utilizing metamaterial in the phone model a SAR value is achieved of about 0.692 W/kg for SAR 10 gm and 1.092 W/kg for SAR 1 gm is achieved. Based on the 3-D FDTD method with lossy-Drude model, it is established that for the both cases of peak SAR 1 gm and SAR 10 gm of the head can be abridged by placing metamaterials among the antenna and the human head. Numerical results can give useful information in designing communication equipment for wellbeing acquiescence.

REFERENCES

1. IEEE C95.1-2005, "IEEE standards for safety levels with respect to human exposure to radio frequency electromagnetic fields, 3 kHz to 300 GHz," Institute of Electrical and Electronics Engineers, New York Inc., NY, 2005.
2. International Non-Ionizing Radiation Committee of the International Radiation Protection Association, "Guidelines on limits on exposure to radio frequency electromagnetic fields in the frequency range from 100 kHz to 300 GHz," *Health Physics*, Vol. 54, No. 1, 115–123, 1988.

3. Wang, J. and O. Fujiwara, "FDTD computation of temperature rise in the human head for portable telephones," *IEEE Trans. on Microwave Theory and Tech.*, Vol. 47, No. 8, 1528–1534, Aug. 1999.
4. Kusuma, A. H., A.-F. Sheta, I. Elshafiey, Z. Siddiqui, M. A. S. Alkanhal, S. Aldosari, S. A. Alshebeili, and S. F. Mahmoud, "A new low SAR antenna structure for wireless handset applications," *Progress In Electromagnetics Research*, Vol. 112, 23–40, 2011.
5. Zhang, M. and A. Alden, "Calculation of whole-body SAR from a 100 MHz dipole antenna," *Progress In Electromagnetics Research*, Vol. 119, 133–153, 2011.
6. Islam, M. T., M. R. I. Faruque, and N. Misran, "Design analysis of ferrite sheet attachment for SAR reduction in human head," *Progress In Electromagnetics Research*, Vol. 98, 191–205, 2009.
7. Yanase, K. and A. Hirata, "Effective resistance of grounded humans for whole-body averaged SAR estimation at resonance frequencies," *Progress In Electromagnetics Research B*, Vol. 35, 15–27, 2011.
8. Manapati, M. B. and R. S. Kshetrimayum, "SAR reduction in human head from mobile phone radiation using single negative metamaterials," *Journal of Electromagnetic Waves and Applications*, Vol. 23, No. 10, 1385–1395, 2009.
9. Hawang, J. N. and F.-C. Chen, "Reduction of the peak SAR in the human head with metamaterials," *IEEE Trans. on Antenna and Propagation*, Vol. 54, No. 12, 3763–3770, Dec. 2006.
10. Naqvi, A., S. Ahmed, and Q. A. Naqvi, "Perfect electromagnetic conductor and fractional dual interface placed in a chiral nihility medium," *Journal of Electromagnetic Waves and Applications*, Vol. 24, Nos. 14–15, 1991–1999, 2010.
11. Pendry, J. B., A. J. Holen, D. J. Robbins, and W. J. Stewart, "Magnetism from conductors and enhanced nonlinear phenomena," *IEEE Trans. on Microwave Theory and Tech.*, Vol. 47, No. 11, 2075–2084, Nov. 1999.
12. Smith, D. R., et al., "Composite medium with simultaneously negative permeability and permittivity," *Phys. Rev. Lett.*, Vol. 84, No. 18, 4184–4187, 2000.
13. Khan, S. N., X. Liu, L. Shao, and Y. Wang, "Complementary split ring resonators of large stop bandwidth," *Progress In Electromagnetics Research Letters*, Vol. 14, 127–132, 2010.
14. Wu, Z., B. Q. Zeng, and S. Zhong, "A double-layer chiral

- metamaterial with negative index,” *Journal of Electromagnetic Waves and Applications*, Vol. 24, No. 7, 983–992, 2010.
15. Sabah, C., “Novel, dual band, single and double negative metamaterials: Nonconcentric delta loop resonators,” *Progress In Electromagnetics Research B*, Vol. 25, 225–239, 2010.
 16. Tay, R. Y. S., Q. Balzano, and N. Kuster, “Dipole configuration with strongly improved radiation efficiency for hand-held transceivers,” *IEEE Trans. on Antennas and Propagat.*, Vol. 46, No. 6, 798–806, Jun. 1998.
 17. Kuo, C.-M. and C.-W. Kuo, “SAR distribution and temperature increase in the human head for mobile communication,” *IEEE Antennas and Propagation Society Int. Symp. Dig.*, 1025–1028, Columbus, OH, 2003.
 18. Faruque, M. R. I., M. T. Islam, and N. Misran, “Analysis of electromagnetic absorption in the mobile phones using metamaterials,” *Electromagnetics Journal*, Vol. 31, No. 3, 215–232, 2011.
 19. Ziolkowski, R. W., “Design, fabrication, and testing of double negative metamaterials,” *IEEE Trans. on Antennas and Propagat.*, Vol. 51, No. 7, 1516–1529, Jul. 2003.
 20. Kuo, C.-W., S.-Y. Chen, Y.-D. Wu, and M.-H. Chen, “Analyzing the multilayer optical planar waveguides with double-negative metamaterial,” *Progress In Electromagnetics Research*, Vol. 110, 163–178, 2010.
 21. Hasar, U. C. and J. J. Barroso, “Retrieval approach for determination of forward and backward wave impedances of bianisotropic metamaterials,” *Progress In Electromagnetics Research*, Vol. 112, 109–124, 2011.
 22. Cao, W. Q., B. N. Zhang, T. B. Yu, A. J. Liu, S. J. Zhao, D. S. Guo, and Z. D. Song, “Single-feed dual-band dual-mode and dual-polarized microstrip antenna based on metamaterial structure,” *Journal of Electromagnetic Waves and Applications*, Vol. 25, No. 13, 1909–1919, 2011.
 23. Choi, J. and C. Seo, “High-efficiency wireless energy transmission using magnetic resonance based on negative refractive index metamaterial,” *Progress In Electromagnetics Research*, Vol. 106, 33–47, 2010.
 24. Alhawari, A. R. H., A. Ismail, M. A. Mahdi, and R. S. A. Raja Abdullah, “Development of novel tunable dual-band negative index metamaterial using open stub-loaded stepped-impedance resonator,” *Progress In Electromagnetics Research B*, Vol. 35, 111–131, 2011.

25. Bayindir, M., K. Aydin, and E. Ozbay, "Transmission properties of composite metamaterials in free space," *Appl. Phys. Lett.*, Vol. 81, No. 1, 120–122, Jul. 2002.
26. Araujo, M. G., J. M. Taboada, J. Rivero, and F. Obelleiro, "Comparison of surface integral equations for left-handed materials," *Progress In Electromagnetics Research*, Vol. 118, 425–440, 2011.
27. Sajin, G. I., "Impedance measurement of millimeter wave metamaterial antennas by transmission line stubs," *Progress In Electromagnetics Research Letters*, Vol. 26, 59–68, 2011.
28. Sievenpiper, D., "High-impedance electromagnetic surfaces with a forbidden frequency band," *IEEE Trans. on Microwave Theory and Tech.*, Vol. 47, 2059–2074, Nov. 1999.
29. Islam, M. T., M. R. I. Faruque, and N. Misran, "Reduction of specific absorption rate (SAR) in the human head with ferrite material and metamaterial," *Progress In Electromagnetics Research C*, Vol. 9, 47–58, 2009.
30. Petrillo, L., F. Jangal, M. Darces, J.-L. Montmagnon, and M. Helier, "Negative permittivity media able to propagate a surface wave," *Progress In Electromagnetics Research*, Vol. 115, 1–10, 2011.
31. Tang, M. C., S.-Q. Xiao, T. Deng, D. Wang, and B.-Z. Wang, "A dual-band epsilon-negative material design using folded-wire structures," *Journal of Electromagnetic Waves and Applications*, Vol. 25, Nos. 2–3, 327–337, 2011.
32. Li, M., H.-L. Yang, X.-W. Hou, Y. Tian, and D.-Y. Hou, "Perfect metamaterial absorber with dual bands," *Progress In Electromagnetics Research*, Vol. 108, 37–49, 2010.
33. Zhao, X., L. Zhao, K. Huang, and C. Liu, "A circularly polarized array composed of linear polarized microstrip patches fed by metamaterial transmission line," *Journal of Electromagnetic Waves and Applications*, Vol. 25, Nos. 11–12, 1545–1553, 2011.
34. Ishikawa, A., T. Tanaka, and S. Kawata, "Negative magnetic permeability in the visible light region," *Phys. Rev. Lett.*, Vol. 95, No. 23, 237401, 2005.
35. Zhou, J., T. Koschny, M. Kafesaki, E. N. Economou, J. B. Pendry, and C. M. Soukoulis, "Saturation of the magnetic response of splitting resonators at optical frequencies," *Phys. Rev. Lett.*, Vol. 95, No. 22, 223902, Nov. 25, 2005.